

1 **Origin of elemental carbon in snow from Western Siberia**  
2 **and northwestern European Russia during winter–spring**  
3 **2014, 2015 and 2016**

4  
5 **Nikolaos Evangeliou<sup>1,\*</sup>, Vladimir P. Shevchenko<sup>2</sup>, Karl Espen Yttri<sup>1</sup>, Sabine**  
6 **Eckhardt<sup>1</sup>, Espen Sollum<sup>1</sup>, Oleg S. Pokrovsky<sup>3,4</sup>, Vasily O. Kobelev<sup>5</sup>, Vladimir B.**  
7 **Korobov<sup>6</sup>, Andrey A. Lobanov<sup>5</sup>, Dina P. Starodymova<sup>2</sup>, Sergey N. Vorobiev<sup>7</sup>,**  
8 **Rona L. Thompson<sup>1</sup>, Andreas Stohl<sup>1</sup>**

9  
10 <sup>1</sup> NILU - Norwegian Institute for Air Research, Department of Atmospheric and Climate  
11 Research (ATMOS), Kjeller, Norway.

12 <sup>2</sup> Shirshov Institute of Oceanology, Russian Academy of Sciences, Nakhimovsky prospect 36,  
13 117997 Moscow, Russia.

14 <sup>3</sup> Geosciences Environment Toulouse, UMR 5563 CNRS, University of Toulouse, 14 Avenue  
15 Edouard Belin, 31400, Toulouse, France.

16 <sup>4</sup> N. Laverov Federal Center for Integrated Arctic Research, Russian Academy of Science,  
17 Sadovaya street, 3, 163000, Arkhangelsk, Russia.

18 <sup>5</sup> Arctic Research Center of the Yamalo-Nenets autonomous district, Vos'moy proezd, NZIA  
19 building, 629730, Nadym, Yamalo-Nenets autonomous district, Russia.

20 <sup>6</sup> North-Western Branch of Shirshov Institute of Oceanology, Russian Academy of Sciences,  
21 Naberezhnaya Severnoy Dviny 112/3, 163061, Arkhangelsk, Russia.

22 <sup>7</sup> BIO-GEO-CLIM Laboratory, Tomsk State University, 36 Prospect Lenina, 634050, Tomsk,  
23 Russia.

24  
25 \*Correspondence to: N. Evangeliou, NILU - Norwegian Institute for Air Research,  
26 Department of Atmospheric and Climate Research (ATMOS), Kjeller, Norway  
27 ([Nikolaos.Evangeliou@nilu.no](mailto:Nikolaos.Evangeliou@nilu.no))

28

29 **Abstract**

30 Short-lived climate forcers have been proven important both for the climate and human  
31 health. In particular, black carbon (BC) is an important climate forcer both as an aerosol and  
32 when deposited on snow and ice surface, because of its strong light absorption. This paper  
33 presents measurements of elemental carbon (EC; a measurement-based definition of BC) in  
34 snow collected from Western Siberia and northwestern European Russia during 2014, 2015  
35 and 2016. The Russian Arctic is of great interest to the scientific community due to the large  
36 uncertainty of emission sources there. We have determined the major contributing sources of  
37 BC in snow in Western Siberia and northwestern European Russia using a Lagrangian  
38 atmospheric transport model. For the first time, we use a recently developed feature that  
39 calculates deposition in backward (so-called retroplume) simulations allowing estimation of  
40 the specific locations of sources that contribute to the deposited mass.

41 EC concentrations in snow from Western Siberia and northwestern European Russia  
42 were highly variable depending on the sampling location. Modelled BC and measured EC  
43 were moderately correlated ( $R = 0.53 - 0.83$ ) and a systematic region-specific model  
44 underestimation was found. Modelled underestimated observations by 42% (RMSE =  $49 \text{ ng g}^{-1}$ )  
45 in 2014, 48% (RMSE =  $37 \text{ ng g}^{-1}$ ) in 2015 and 27% (RMSE =  $43 \text{ ng g}^{-1}$ ) in 2016. For EC  
46 sampled in northwestern European Russia the underestimation by the model was smaller  
47 (fractional bias,  $\text{FB} > -100\%$ ). In this region, the major sources were transportation activities  
48 and domestic combustion in Finland. When sampling shifted to Western Siberia, the model  
49 underestimation was more significant ( $\text{FB} < -100\%$ ). There, the sources included emissions  
50 from gas flaring as a major contributor to snow BC. The accuracy of the model calculations  
51 was also evaluated using two independent datasets of BC measurements in snow covering the  
52 entire Arctic. The model underestimated BC concentrations in snow especially for samples  
53 collected in springtime.

54

## 55 **1 Introduction**

56 Black carbon (BC) is the strongest light-absorbing component of atmospheric aerosol  
57 and is formed by the incomplete combustion of fossil fuels, biofuels, and biomass (Bond et  
58 al., 2013). It is emitted directly into the atmosphere in the form of fine particles. BC is a major  
59 component of “soot”, a complex light-absorbing mixture that also contains organic carbon  
60 (OC) (Bond et al., 2004). Combustion sources emitting BC include open biomass burning  
61 (forest, savanna, agricultural burning), residential biofuel combustion, diesel engines for  
62 transportation or industrial use, industrial processes and power generation, or residential coal  
63 combustion (Liu et al., 2011; Wang et al., 2011).

64 BC is important on a global perspective because of its impacts on human health and on  
65 climate. As a component of fine particulate matter (PM<sub>2.5</sub>), it is associated with negative  
66 health impacts, including premature mortality (Lelieveld et al., 2015; Turner et al., 2005). It  
67 absorbs solar radiation, has a significant impact on cloud formation and, when deposited on  
68 ice and snow, it accelerates ice melting (Hansen and Nazarenko, 2004). BC has a lifetime that  
69 can be as long as 9–16 days (Bond et al., 2013). After its emission, BC can travel over long  
70 distances (Forster et al., 2001; Stohl et al., 2006) and reach remote areas such as the Arctic.  
71 Arctic land areas are covered by snow in winter and spring, while the Arctic Ocean is partly  
72 covered by ice. Sea ice has a much higher albedo ( $\approx 0.5$ – $0.7$ ) compared to the surrounding  
73 ocean ( $\approx 0.06$ ), thus presence of sea ice reduces the heat uptake of the ocean. Snow has an  
74 even higher albedo than sea ice and can reflect as much as 90% of the incoming solar  
75 radiation (Brandt et al., 2005; Singh and Haritashya, 2011). BC deposited on ice lowers its  
76 albedo, increases heat uptake by sea ice, accelerates its melting, and therefore decreases  
77 surface albedo both directly and indirectly.

78 Hegg et al. (2009) reported that snow in the Arctic often contains BC at concentrations  
79 between 1 and 30 ng g<sup>-1</sup>, which can cause a snow albedo reduction of 1–3% in fresh snow and  
80 another 3–9% as snow ages and BC becomes more concentrated near the surface (Clarke and  
81 Noone, 1985). This solar radiation reflecting capacity of snow insulates the sea ice, maintains  
82 cold temperatures and delays ice melt in summertime. After the snow begins to melt and  
83 because shallow melt ponds have an albedo of approximately 0.2 to 0.4, the surface albedo  
84 drops to about 0.75 or even lower (0.15) as melt ponds grow and deepen (Singh and  
85 Haritashya, 2011). These changes have been found to be important for the global energy

86 balance (Flanner et al., 2007; Hansen and Nazarenko, 2004) and, if enhanced by BC,  
87 contribute to climate warming (Warren and Wiscombe, 1980).

88 Although BC in Arctic snow and ice has been found to be important for the Earth's  
89 climate (Flanner et al., 2007; Sand et al., 2015), its large-scale temporal and spatial  
90 distributions and exact origin are still poorly quantified (AMAP, 2015). Efforts to determine  
91 the concentrations of BC in snow across the Arctic were made by Clarke and Noone (1985),  
92 Doherty et al. (2010, 2013), Forsström et al. (2013), Ingvander et al. (2013) and McConnell et  
93 al. (2007). This paper presents measurements of Elemental Carbon (EC) concentrations in  
94 snow samples collected in spring 2014, 2015 and 2016 in the Kindo Peninsula (White Sea,  
95 Karelia), around Arkhangelsk in northwestern European Russia, and in Western Siberia. In  
96 the latter area, gas flaring emissions are very important. Flaring emissions are highly  
97 uncertain because both activity data and emission factors are largely lacking. According to the  
98 Global Gas Flaring Reduction Partnership (GGFR)  
99 (<http://www.worldbank.org/en/programs/gasflaringreduction>), nearly 50 billion m<sup>3</sup> of gas are  
100 flared in Russia annually. The Russian flaring emissions in the Nenets/Komi regions and in  
101 Khanty-Mansiysk are the major sources in Western Siberia and northwestern European  
102 Russia. It has been reported that gas flaring in Russia contributes about 42% to the annual  
103 average BC surface concentrations in the Arctic (Stohl et al., 2013).

104 The use of the terms EC and BC has been the topic of several scientific papers (for  
105 example, Andreae and Gelencsér, 2006; Bond et al., 2013; Petzold et al., 2013). Petzold et al.  
106 (2013) defined BC as a substance with 5 properties (see Table 1 in Petzold et al., 2013), for  
107 which no single measurement instrument exists that is sensitive to all of them at the same  
108 time. Consequently, BC cannot uniquely be measured, although some of its properties can,  
109 such as the absorption coefficient  $\sigma_{ap}$  and the elemental carbon (EC) concentration, both  
110 commonly measured in atmospheric monitoring networks across the world. Hence, the term  
111 BC should be used qualitatively.

112 In the present study, EC concentrations on ice from three campaigns measured with  
113 Thermal–Optical Analysis (TOA) (see section 2.2) are compared to simulation results from  
114 the Lagrangian particle dispersion model (LPDM) FLEXPART. The model is used here for  
115 the first time to quantify the sources contributing to BC in snow in Russia adopting a special  
116 feature that was developed recently.



## 117 **2 Methodology**

### 118 **2.1 Collection and storage of snow samples**

119 Fresh snow samples were collected along a north–south transect between Tomsk and  
120 the Yamal coast in February–March 2014 (23 samples, Table S 1), while in March 2015  
121 sample collection took place in the Kindo Peninsula and near the port of Arkhangelsk in the  
122 White Sea (11 samples, Table S 1). Finally, in February–May 2016 samples were collected in  
123 the Kindo Peninsula, in Arkhangelsk and between Tomsk and Yamal (20 samples, Table S 1).  
124 These areas have been reported to receive pollution both from urban and gas flaring sources  
125 (Stohl et al., 2013). For example, the gas flaring sources located in Yamal and Khanty-  
126 Mansiysk (Russia) are in the main pathway along which sub-Arctic air masses travel to the  
127 Arctic (Stohl et al., 2006). All sampling points were located more than 500 m away from  
128 roads to minimize the direct influence from local traffic emissions. Information about sample  
129 collection such as the location of sampling, the amount of snow collected and the depth at  
130 which snow was sampled is reported in Table S 1 and the sample locations are plotted in  
131 Figure 1.

132 Sampling was performed using a metal-free technique using pre-cleaned plastic shovels  
133 and single–use vinyl gloves. Samples were stored in polyethylene bags which had been  
134 thoroughly washed with 1 M HCl and rinsed with abundant deionised ultrapure water in the  
135 laboratory prior to their use. After returning the samples to the laboratory, the snow was  
136 allowed to melt at ambient temperature (18–20°C), and immediately filtered through quartz  
137 47 mm fibre filters (2500QAT-UP Pall for samples collected in 2014 and QM-A Whatman for  
138 samples collected in 2015 and 2016). The filters were dried at 60–70°C, wrapped in  
139 aluminum foil and stored in a refrigerator. Quartz fiber filter collection efficiency of BC in  
140 liquid samples can be less than 100% (Hadley et al., 2010; Ogren et al., 1983). To what extent  
141 this has affected the levels reported in the present study is unknown. Thus the results  
142 presented should be regarded as conservative estimates based on the assumption that some  
143 BC might have been lost during filtration.

### 144 **2.2 Elemental Carbon measurements by Thermal–Optical Analysis (TOA)**

145 Elemental carbon (EC) content of the filters was measured at NILU’s laboratories by thermal-  
146 optical analysis (TOA), using the Sunset laboratory OC/EC instrument operated according to  
147 the EUSAAR-2 protocol (Cavalli et al., 2010). A 1.5 cm<sup>2</sup> punch was cut from the filtered  
148 snow samples for the analysis. Transmission was used for organic carbon (OC) charring

149 correction. Performance of the OC/EC instrument's is regularly intercompared as part of the  
150 joint European Monitoring and Evaluation Programme (EMEP) Aerosols, Clouds, and Trace  
151 gases Research InfraStructure Network (ACTRIS) quality assurance and quality control effort  
152 (Cavalli et al., 2015).

### 153 **2.3 Measurements of carbonate ( $CO_3^{2-}$ )–carbon by Thermal–Optical Analysis** 154 **(TOA) following thermal-oxidative pre-treatment**

155 The content of carbonate ( $CO_3^{2-}$ )–carbon on the filters was measured by TOA,  
156 following thermal-oxidative pretreatment based on the approach described by Jankowski et al.  
157 (2008). A punch of 1.5 cm<sup>2</sup> from each filter was heated at 450 °C for 2 hours in ambient air to  
158 remove OC and EC, but not  $CO_3^{2-}$ –carbon. The filter punch was subjected to TOA  
159 immediately (30 sec) after thermal-oxidative pre-treatment. The split time (between OC and  
160 EC) obtained for each filter punch used to determine the filter samples' content of EC (section  
161 2.2) was also used to apportion  $CO_3^{2-}$ –carbon to OC and/or EC. The influence of  $CO_3^{2-}$ –  
162 carbon evolving as EC, was accounted for by the following equation:

$$EC_{CO_3^{2-}}^{corr} = EC - EC_{CO_3^{2-}}$$

163 where  $EC_{CO_3^{2-}}^{corr}$  is elemental carbon corrected for  $CO_3^{2-}$ –carbon that evolved as EC during  
164 TOA, EC is elemental carbon and  $EC_{CO_3^{2-}}$  is  $CO_3^{2-}$ –carbon that evolved as EC during TOA.  
165 Applying this correction, EC values were 5-22% lower (see Supplementary Information).

### 166 **2.4 Emissions and modelling of black carbon**

167 The concentrations of BC in snow were simulated with the LPDM FLEXPART version  
168 10 (Stohl et al., 1998, 2005). The model was driven with operational meteorological wind  
169 fields retrieved from the European Centre for Medium-Range Weather Forecasts (ECMWF)  
170 of 3–hour (for the years 2014 and 2015) and hour (for the year 2016) temporal resolution. The  
171 ECMWF data have 137 vertical levels and a horizontal resolution of 1°×1° for the 2014 and  
172 2015 simulations and 0.5°×0.5° for the 2016.

173 The simulations were conducted in backwards time (“retroplume”) mode, using a new  
174 feature of FLEXPART to reconstruct wet and dry deposition with backward simulations  
175 (Eckhardt et al., 2017). This new feature is an extension of the traditional possibility to  
176 simulate atmospheric concentrations backward in time (Seibert and Frank, 2004; Stohl et al.,  
177 2003). It is computationally efficient because it requires only two single tracer transport

178 simulations (one for wet deposition, one for dry deposition) for each measurement sample. To  
179 reconstruct wet deposition amounts of BC, computational particles were released at altitudes  
180 of 0 to 20 km at the locations where snow samples were taken, whereas to reconstruct dry  
181 deposition, particles were released between the surface and 30 m at these locations. All  
182 released particles represent a unity deposition amount, which was converted immediately (i.e.,  
183 upon release of a particle) to atmospheric concentrations using the deposition intensity as  
184 characterized either by dry deposition velocity or scavenging rate (for further details, see  
185 Eckhardt et al., 2017). The concentrations were subsequently treated as in normal  
186 “concentration mode” backward tracking (Seibert and Frank, 2004) to establish source-  
187 receptor relationships between the emissions and deposition amounts. The termination time of  
188 the particle release was the time at which the snow sample was collected, whereas the  
189 beginning time was set as the time when the ECMWF precipitation at the sampling site,  
190 accumulated backward in time, was equal to the water equivalent of the snow sample, up to  
191 the specified sampling depth.

192 The model output consists of a spatially gridded sensitivity of the BC deposition at the  
193 sampling location (receptor) to the BC emissions, equivalent to the backwards time mode  
194 output for concentrations (Seibert and Frank, 2004; Stohl et al., 2003). BC deposition at the  
195 snow sampling point can be computed (in mass per unit area) by multiplying the emission  
196 sensitivity in the lowest model layer (the footprint emission sensitivity) with gridded  
197 emissions from a BC emission inventory and integrating over the grid. The deposited BC can  
198 be easily converted to BC snow concentration by taking into account the water equivalent  
199 depth of the snow from ECMWF (in mm). In the present study, the ECLIPSE (Evaluating the  
200 CLimate and Air Quality ImPacts of ShortlivEd Pollutants) version 5 emission inventory  
201 (Klimont et al., 2016; Stohl et al., 2015) was used  
202 ([http://www.iiasa.ac.at/web/home/research/researchPrograms/air/Global\\_emissions.html](http://www.iiasa.ac.at/web/home/research/researchPrograms/air/Global_emissions.html)).  
203 The total emissions of BC from ECLIPSE in the areas of study are shown in Figure 1 (left  
204 panel).

205 BC was assumed to have a density of  $2 \text{ g m}^{-3}$  in our simulations and a logarithmic size  
206 distribution with an aerodynamic mean diameter of  $0.25 \text{ }\mu\text{m}$  and a logarithmic standard  
207 deviation of 0.3. Each computational particle released in FLEXPART represents an aerosol  
208 population with a lognormal size distribution (see Stohl et al., 2005). Assumed aerodynamic  
209 mean diameter and logarithmic standard deviation are used by FLEXPART’s dry deposition  
210 scheme, which is based on the resistance analogy (Slinn 1982), and they are consistent with

211 those used in other transport models (see Evangeliou et al., 2016; Shiraiwa et al., 2008).  
212 Below-cloud scavenging was determined based on the precipitation rate taken from ECMWF.  
213 The in-cloud scavenging was based on cloud liquid water and ice content, precipitation rate  
214 and cloud depth from ECMWF (Grythe et al., 2017). The FLEXPART user manual (available  
215 from <http://www.flexpart.eu>) provides more information. All modelling results for this  
216 sampling campaign can be viewed interactively at the URL  
217 [http://niflheim.nilu.no/NikolaosPY/SnowBC\\_141516.py](http://niflheim.nilu.no/NikolaosPY/SnowBC_141516.py).

### 218 3 Results

219 In this section the main results of EC concentrations in snow are presented, in contrast  
220 to simulated BC concentrations with FLEXPART. The statistical dependence of the datasets  
221 is assessed using the Pearson product-moment correlation coefficient. For further validation,  
222 the fractional bias (FB) of each individual sample was calculated together with the mean  
223 fractional bias (MFB) for observed and modelled concentrations as follows:

$$FB = \frac{C_m - C_o}{(C_m + C_o)/2} \times 100\% \text{ and } MFB = \frac{1}{N} \sum_{i=1}^N \frac{C_m - C_o}{(C_m + C_o)/2} \times 100\%$$

224 where  $C_m$  and  $C_o$  are the modelled BC and measured EC concentrations and  $N$  is the total  
225 number of observations for each year. FB is a useful model performance indicator because it  
226 is symmetric and gives equal weight to underestimations and overestimations (it takes values  
227 between -200% and 200%). It is used here to show the locations where modelled BC  
228 concentrations in snow over- or underestimate observations. Finally, for the same reasons, the  
229 root mean square error (RMSE) was also computed, which is frequently used to measure  
230 differences between values predicted by a model and the values actually observed (see Figure  
231 S 1 – S 3).

#### 232 3.1 Elemental Carbon concentrations measured in snow

233 The spatial distribution of EC measured in snow samples from northwestern European  
234 Russia and Western Siberia is shown in Figure 1(c) for each of the campaigns (2014, 2015  
235 and 2016) and are also summarised in Table S 2. There was large spatial variability in the  
236 distribution of EC in snow in 2014 ranging from 3 to 219 ng g<sup>-1</sup>, with a median (±interquartile  
237 range) of 23±49 ng g<sup>-1</sup>. The highest EC concentrations in 2014 were observed in Western  
238 Siberia near Tomsk (147 to 219 ng g<sup>-1</sup>). FLEXPART emission sensitivities for these samples

239 showed that the air was coming from the north and the east (see in  
240 [http://niflheim.nilu.no/NikolaosPY/SnowBC\\_141516.py](http://niflheim.nilu.no/NikolaosPY/SnowBC_141516.py)). This explains the high  
241 concentrations of EC, as most of the anthropogenic BC sources are located in these regions.  
242 In the rest of the snow samples for 2014, EC concentrations between 4 and 170 ng g<sup>-1</sup> were  
243 observed. High concentrations were observed near the Ob River coinciding with air masses  
244 arriving mainly from Europe. During the 2015 field campaign, EC concentrations were the  
245 highest near Arkhangelsk (175 ng g<sup>-1</sup>), for which FLEXPART showed that the air was coming  
246 from nearby areas ([http://niflheim.nilu.no/NikolaosPY/SnowBC\\_141516.py](http://niflheim.nilu.no/NikolaosPY/SnowBC_141516.py)). Therefore, it is  
247 likely that the samples were affected by direct emissions from the city or the port of  
248 Arkhangelsk. During the same campaign, snow samples collected in the Kindo peninsula (on  
249 the White Sea coast) showed high variability in EC concentrations (range: 46 – 152 ng g<sup>-1</sup>,  
250 median=70±34 ng g<sup>-1</sup>). According to FLEXPART emission sensitivities, air masses were  
251 transported to Kindo peninsula from central and southern Europe driven by an anticyclone  
252 over Scandinavia ([http://niflheim.nilu.no/NikolaosPY/SnowBC\\_141516.py](http://niflheim.nilu.no/NikolaosPY/SnowBC_141516.py)). Finally, for the  
253 snow samples collected outside Arkhangelsk, at the Kindo peninsula, and close to the Yamal  
254 Peninsula in Western Siberia in 2016, EC concentrations ranged between 7–161 ng g<sup>-1</sup>  
255 (median: 40±47 ng g<sup>-1</sup>). Outside Arkhangelsk, EC concentrations varied widely from 31 to  
256 161 ng g<sup>-1</sup> with a median concentration in this region of 61±43 ng g<sup>-1</sup>. This is far below the  
257 175 ng g<sup>-1</sup> observed in 2015, although there was only one sample collected in that year. In the  
258 Kindo Peninsula, EC was relatively constant in 2016 ranging between 25 and 35 ng g<sup>-1</sup>  
259 (median = 28±4 ng g<sup>-1</sup>), which is more than 60% lower compared with the 2015 values  
260 (median = 70±34 ng g<sup>-1</sup>). Finally, between Tomsk and Yamal, EC concentration was highly  
261 variable (7 – 119 ng g<sup>-1</sup>) due to the different EC sources affecting snow (median = 50±34 ng  
262 g<sup>-1</sup>). For instance, it is expected that gas flaring affects snow close to Yamal, while snow  
263 collected in the south (Tomsk) is likely influenced by sources in Europe or local urban  
264 emissions. Nevertheless, the highest concentrations (>100 ng g<sup>-1</sup>) were observed north of  
265 68°N, in the Yamal Peninsula.

266 We compared the measured EC concentrations in the snow samples with those  
267 calculated by FLEXPART. For this, the emission sensitivities were multiplied with the total  
268 emission fluxes from ECLIPSE (section 2.4). A scatter plot of modelled and measured snow  
269 concentrations is presented in Figure 1 (b). The results show a good correlation between  
270 modelled BC and measured EC concentrations for the 2015 and 2016 campaigns ( $R_{2015} =$   
271  $0.83$  and  $R_{2016} = 0.68$ ,  $p - value < 0.05$ ), but weaker correlation for 2014 ( $R_{2014} = 0.53$ ,

272  $p - value < 0.05$ ). The FB for individual samples is shown in Figure S 1. The MFB of the  
273 model for the 2014 snow measurements was  $-42\%$ , which shows that the model  
274 underestimated observations. In total, the model underestimated concentrations by  $30\% -$   
275  $168\%$  for 17 out of 23 samples, whereas for the rest (six samples) FB values ranged between  
276  $20\%$  and  $148\%$  (median MFB:  $-56\% \pm 72\%$ ) (Figure S 1). In 2015, the model underestimated  
277 observations by  $48\%$  (median MFB:  $-56\% \pm 29\%$ ) for 11 out of 12 samples (FB between  $-$   
278  $101\%$  and  $-7\%$ , while one value was found to be  $12\%$ ). For 2016, FB values of the simulated  
279 concentrations of BC in snow showed another set of underestimation (median:  $-13\% \pm 60\%$ )  
280 between  $0.3\%$  and  $198\%$  for 12 out of 19 samples. For the remaining seven samples, the  
281 model predicted higher concentrations compared with observations ( $10\%$  to  $75\%$ ) (Figure S  
282 1). RMSE values were estimated to be quite high, between  $37$  and  $49 \text{ ng g}^{-1}$ , due to the large  
283 variation of the observed EC concentrations.

284 The levels of EC in snow presented here are relatively high compared to previously  
285 reported concentrations in the Arctic. Apart from Aamaas et al. (2011) who measured  
286 maximum EC concentration in snow close to the airport of Svalbard of more than  $1000 \text{ ng g}^{-1}$ ,  
287 most of the reported levels of EC in the relevant literature are close to our findings. For  
288 instance, Ruppel et al. (2014) found that EC concentrations have been increasing up to  $103 \text{ ng}$   
289  $\text{g}^{-1}$  since 1970 in Svalbard. McConnell et al. (2007) reported that the BC concentrations  
290 measured at the D4 ice-core site in Greenland were  $10 \text{ ng g}^{-1}$ , at maximum, which most likely  
291 originated from biomass burning in the conifer-rich boreal forest of the Eastern and Northern  
292 United States and Canada. Forsström et al. (2013) reported concentrations as high as  $88 \text{ ng g}^{-1}$   
293 in Scandinavia, and lower ones at higher latitudes ( $11-14 \text{ ng g}^{-1}$  in Svalbard,  $7-42 \text{ ng g}^{-1}$  in  
294 the Fram Strait, and  $9 \text{ ng g}^{-1}$  in Barrow). Svensson et al. (2013) collected snow samples from  
295 Tyresta National Park and Pallas-Yllästunturi National Park in Sweden. Tyresta is a relatively  
296 polluted site located circa  $25 \text{ km}$  from the city centre of Stockholm with a population of about  
297  $2$  million people. Yllästunturi National Park is located in Arctic Finland and a clean site with  
298 no major city influencing the local and regional air. The concentration of EC in Pallas-  
299 Yllästunturi was between  $0$  and  $140 \text{ ng g}^{-1}$ , while in Tyresta the BC concentrations were up to  
300 more than  $7$  times higher ( $53-810 \text{ ng g}^{-1}$ ). Furthermore, Doherty et al. (2010) in the most  
301 complete dataset for the Arctic snow and ice BC reported highly variable concentrations (up  
302 to  $800 \text{ ng g}^{-1}$ ) for five consecutive years (2005–2009). Finally, in the most recent dataset for  
303 snow BC, Macdonald et al. (2017) reported BC concentrations ranging from  $0.3$  to  $15 \text{ ng g}^{-1}$   
304 were reported for the samples collected near the Alert observatory (see section 4.1).

## 305 **3.2 Sources and origin of BC**

306 We further analysed the model output in order to calculate relevant contributions from  
307 various BC source types to BC concentrations in snow (for method description, see section  
308 2.4). ECLIPSE emissions include waste burning (WST), industrial combustion and processing  
309 (IND), surface transportation (TRA), power plants, energy conversion, and extraction (ENE),  
310 residential and commercial combustion (DOM), gas flaring (FLR), while biomass burning  
311 (BB) emissions were adopted from the Global Fire Emissions Database, Version 4  
312 (GFEDv4.1) (Giglio et al., 2013). The results are depicted in Figure 2 for the sampling  
313 campaigns of 2014, 2015 and 2016 in Western Siberia and North-Western European Russia,  
314 sorted from the northernmost to the southernmost sampling location.

315 In 2014, TRA contributed about 18%, on average, to the simulated BC in snow, DOM  
316 28%, FLR 44%, whereas ENE and IND were less significant. Maxima of TRA, DOM, and  
317 FLR contributions were observed at a latitude of about 65°N, where measured EC and  
318 modelled BC were similar. An example of the contribution from the aforementioned  
319 dominant sources to snow BC concentrations for the highest measured EC concentration in  
320 snow is shown in Figure 3. The transport sector includes emissions from all land-based  
321 transport of goods, animals and persons. It is more significant in southern Russia and close to  
322 the borders with Kazakhstan and Mongolia, where a large number of major Russian cities  
323 (e.g., Moscow, Kazan, Samara, Yekaterinburg, Tomsk, Novosibirsk, Krasnoyarsk, etc...) are  
324 located and connected with each other by federal highways. Residential and commercial  
325 combustion includes emissions from combustion in households and public and commercial  
326 buildings. Therefore, it is expected to be high for areas that consist of large population centres  
327 (Figure 3). FLR emissions were found to contribute the most in this example with a total  
328 concentration from this sector of 19.7 ng g<sup>-1</sup> (compared with 12.6 and 16.5 ng g<sup>-1</sup> in TRA and  
329 DOM, respectively) (Figure 3).

330 In the Kindo Peninsula and in Arkhangelsk, where snow sampling took place in 2015,  
331 the main contributions to snow BC were from DOM (47%), TRA (30%), BB (7%), and FLR  
332 (6%) (see Figure 2). Similar to EC measurements in snow, simulated BC was also higher than  
333 in 2014, as the sampling sites were located closer to strong sources in Europe (Kindo) and  
334 close to a populated area (Arkhangelsk) with a strong regional impact. The highest  
335 concentration of EC was observed in the Kindo Peninsula (33.13°E – 66.53°N). Figure 4  
336 shows the spatial distribution of emissions that contributed to simulated snow BC at the

337 sampling point where the highest BC concentration was observed. In this case, TRA and  
338 DOM emissions from Europe mostly affected snow in the Kindo Peninsula whereas FLR  
339 emissions were very low due to the long distance from the sampling point. Emissions from an  
340 unusual late winter/early spring episode of BB in the borders of Belarus, Ukraine and Russia  
341 also affected BC concentrations in snow in northwestern European Russia (Figure 4). The  
342 importance of episodic BB releases in Russia, the miscalculation of satellite retrieved BB  
343 emissions and their impact in Arctic concentrations in early spring has been explained by  
344 Evangeliou et al. (2016) and Hao et al. (2016). BB emissions, originating mostly from Eastern  
345 Europe, contributed about  $19.4 \text{ ng g}^{-1}$  to the snow concentration at the receptor point (Figure  
346 4). TRA and DOM emissions were the dominant sources for this sampling point, contributing  
347  $33.6$  and  $47.2 \text{ ng g}^{-1}$ , respectively (Figure 4).

348 Finally, in 2016, when samples were collected at the Kindo Peninsula, in Arkhangelsk  
349 and in Yamal, DOM, FLR and TRA contributed, on average, 31%, 29% and 27%,  
350 respectively (see Figure 2 (c)). Similar to the measured EC concentrations in snow, simulated  
351 concentrations of BC in 2016 were lower than those in 2015, on average. The highest  
352 measured EC concentration was observed in the Khanty-Mansiysk region ( $72.94^{\circ}\text{E} -$   
353  $65.36^{\circ}\text{N}$ ), which mirrors the simulated BC concentration at the same point very well. The  
354 much higher contribution from TRA at this sampling point ( $38.6 \text{ ng g}^{-1}$ ) (Figure 5 (b)) is  
355 attributed to emissions from Southern Russia (e.g., Tomsk), where all the main cities in  
356 Russia are located. Another large fraction of TRA emissions comes from Central and Eastern  
357 Europe (see also in [http://niflheim.nilu.no/NikolaosPY/SnowBC\\_141516.py](http://niflheim.nilu.no/NikolaosPY/SnowBC_141516.py)). Similar to  
358 TRA, emissions from DOM were mostly transported to Khanty-Masiysk from Central and  
359 Eastern Europe, as well as from Turkey contributing  $36.6 \text{ ng g}^{-1}$  (Figure 5). As previously  
360 mentioned, the sampling point where the highest EC concentration was measured is located  
361 inside the largest gas flaring region of Russia. In addition, the corresponding emission  
362 sensitivity maps showed that the air was coming from south passing directly through this high  
363 emission region making FLR emissions the highest contributing source ( $88.8 \text{ ng g}^{-1}$ ) (Figure  
364 5).

## 365 **4 Discussion**

### 366 **4.1 Cross validation of modelled BC concentrations with public datasets**

367 In this section, we present an effort to further validate our model calculations of BC  
368 concentrations in snow. For this purpose, BC concentrations in snow that were adopted from



369 Doherty et al. (2010) were compared with modelled BC concentrations in snow that were  
370 simulated with FLEXPART as described in section 2.4. Samples were collected in Alaska,  
371 Canada, Greenland, Svalbard, Norway, Russia, and the Arctic Ocean during 2005–2009, on  
372 tundra, glaciers, ice caps, sea ice, frozen lakes, and in boreal forests. Snow was collected  
373 mostly in spring, when the combination of snow cover and exposure to sunlight is at  
374 maximum and before the snow had started to melt. Samples of melting snow collected in the  
375 summer of 2008 from Greenland and from Tromsø, Norway, were removed from the study, as  
376 we have no knowledge about the depth of the melt layer and effects of the percolation of  
377 meltwater through the snowpack. All samples were collected away from local sources of  
378 pollution. In many locations (Canadian Arctic, Russia, Greenland, Tromsø and Ny-Ålesund)  
379 samples were gathered at different depths throughout the snowpack, giving information on the  
380 seasonal evolution of BC concentrations as the snow accumulated (and/or sublimated)  
381 throughout the winter. In these cases only the surface BC was taken into account. The snow  
382 was melted and filtered, and the filters were analysed in a specially designed  
383 spectrophotometer system to infer the concentration of BC (for more information see Doherty  
384 et al., 2010). In contrast to our findings for the origin of snow BC in the Russian Arctic, a  
385 source apportionment analysis performed in the 2008 and 2009 measurements (Hegg et al.,  
386 2010) from this dataset showed that the dominant source of BC in the Arctic snow pack was  
387 biomass burning. Specifically in Eastern Siberia biomass burning of crops and grasslands  
388 contributed more snow BC in high latitudes than boreal forest fires, in contrast to the  
389 Canadian Arctic.

390 A comparison of modelled (FLEXPART) and measured BC concentrations (Doherty et  
391 al., 2010) in snow is depicted in Figure S 2. The model captures snow BC concentrations  
392 relatively well in most of the Arctic regions except for the Canadian Arctic, where the  
393 modelled concentrations of snow in 2007 were significantly higher. Samples from the same  
394 region in other years showed moderate agreement with modelled values. Similar to our  
395 finding for the new Russian measurements, the model underestimated deposition by 51%. The  
396 RMSE was estimated to be  $52 \text{ ng g}^{-1}$ , which is acceptable considering that the variation of  
397 snow concentrations in the dataset ranged from 0.3 to  $783 \text{ ng g}^{-1}$ . The highest measured  
398 concentrations of snow BC were observed in Russia, where the model showed a good spatial  
399 agreement. For instance, the highest values were obtained in Western Siberia, close to the gas  
400 flaring regions of the Nenets/Komi oblast, as well as in southeastern and northeastern Russia,  
401 where air masses were arriving from high emitting sources in southeastern Asia. Lower biases

402 in modelled BC concentrations were observed in northern Siberia with the exception of a few  
403 samples at the coasts of the Kara Sea and northeastern Siberia. Furthermore, biased BC  
404 concentrations were also observed in Greenland and northern Canada. In Western Siberia, BC  
405 in snow presented in Doherty et al. (2010) between 2005–2009 was  $80\pm 63$  ng g<sup>-1</sup> on average,  
406 which is very close to the average value of measured EC obtained from the sampling 2014–  
407 2016 campaigns ( $50\pm 46$  ng g<sup>-1</sup>).

408 From total number of samples presented in (Doherty et al., 2010) that were used here  
409 for validation, only six were collected in the Yamal Peninsula similar as part of the data  
410 presented in the current paper. The rest was collected in Nenets/Komi region and in Eastern  
411 Russia and cannot be directly compared with snow EC measurements from the 2014 – 2016  
412 campaigns. BC concentrations in Yamal Peninsula in 2007 ranged from 4.1 to 17.6 ng g<sup>-1</sup>  
413 (median±interquartile:  $10.3\pm 4.9$  ng g<sup>-1</sup>). In the same region, we report EC concentrations to be  
414 more than double varying between 6.6 to 55 ng g<sup>-1</sup> (median±interquartile:  $27.8\pm 25.5$  ng g<sup>-1</sup>),  
415 whereas there were two samples that showed EC concentrations of more than 100 ng g<sup>-1</sup>. As  
416 mentioned in section 2.1 the sampling of snow for the EC analysis took place more than 500  
417 m away from roads to minimize influence from traffic emissions, while a similar statement is  
418 also found in the Doherty et al. (2010) data. It is not clear whether the observed discrepancy  
419 arises as a measurement artefact (even though every effort has been taken in both papers to  
420 follow a robust protocol) or from real spatio-temporal variation.

421 Modelled BC concentrations simulated with FLEXPART were also compared with  
422 snow BC concentrations from samples collected at the Global Atmosphere Watch  
423 Observatory at Alert, Nunavut, from September 14<sup>th</sup>, 2014 to June 1<sup>st</sup>, 2015 and they are  
424 available in Macdonald et al. (2016). Alert is a remote outpost in the Canadian high Arctic, at  
425 the northern coast of Ellesmere Island (82°27' N, 62°30' W), with a small transient  
426 population of research and military personnel. Sampling details and analytical methodologies  
427 used for the analysis of BC can be found in Macdonald et al. (2016). BC concentrations in  
428 FLEXPART were simulated as in all previous analyses described in this paper (see section  
429 2.4.). Timeseries of simulated and measured BC are depicted in Figure S 3 for the whole  
430 sampling period. As before, a correlation coefficient (*R*) of 0.63 indicates that our model  
431 captures the temporal variation of the measured BC in snow. The RMSE was estimated to be  
432 almost 63 ng g<sup>-1</sup>, a relatively high value. The MFB of 47% indicates a strong overestimation  
433 of snow concentrations, although in many samples the opposite was also observed (Figure S

434 3). This is in contrast to the previous data sets discussed, for which the model underestimated  
435 measurements.

436 Further analysis was carried out to adequately understand the origin of the  
437 aforementioned overestimations in the Canadian Arctic in both datasets (Doherty et al., 2010;  
438 Macdonald et al., 2017), as they are shown to be rather systematic. For this reason, we have  
439 calculated the average footprint emission sensitivities and the average BC contribution from  
440 the major sources in ECLIPSE for the 2007 snow samples in the Canada Arctic and for Alert  
441 samples. We have chosen these samples, because they were three or more times higher than  
442 the observations and in this way we can locate the observed overestimations predicted with  
443 FLEXPART (Figure 6).

444 Regarding the model overestimation for the 2007 samples, the average footprint  
445 emission sensitivity showed that the air was coming from continental regions of Canada with  
446 a smaller contribution from Scandinavia (Figure 6). The highest emission sources for these  
447 samples were TRA and DOM that contributed almost 80% to the snow concentrations,  
448 whereas forest fires were less important at the time of sampling. Two hot spots were  
449 identified, one along the borders of Canada with USA and another, of smaller intensity, in  
450 southeastern Asia. A similar emission sensitivity was obtained for the same area of the  
451 Canadian Arctic in 2009 only slightly shifted to the north; simulated concentrations were in  
452 very good agreement with observations (Figure S 2). This shows that the model  
453 overestimation for the 2007 samples is likely attributed to an overestimation of TRA and  
454 DOM sources in North America in ECLIPSE for 2007. For the Alert samples, for which the  
455 model strongly overestimated BC, the major sources were TRA and FLR, which contributed  
456 55%, and BB which contributed about  $7 \text{ ng g}^{-1}$  (22%) on average (Figure 6). Anthropogenic  
457 BC arriving from Europe and Russia has been previously shown to be important for Alert air  
458 pollutant concentrations (Sharma et al., 2013). The model overestimation of BC in snow  
459 samples at Alert needs further investigation. It is likely that it originates from anthropogenic  
460 emissions in northwestern America or in Europe, because forest fires in Canada and Russia,  
461 although important for Alert (e.g., Qi et al., 2017), were not significant in the present  
462 comparison.

## 463 **4.2 Model deviation from snow EC measurements and region-specific** 464 **contribution of sources**

465 It has been shown that measured concentrations of EC in snow in northwestern  
466 European Russia and Western Siberia were underestimated in FLEXPART (Figure 2). This  
467 was confirmed by the calculated fractional bias (see section 3.2), the spatial distribution of  
468 which is shown in Figure S 1. To examine whether this underestimation was due to missing  
469 emission sources or errors in modelled transport and deposition, we have calculated the  
470 average footprint emission sensitivity for those sampling points, for which FLEXPART  
471 strongly ( $FB < -100\%$ ) and slightly ( $-100\% < FB < 0\%$ ) underestimated the observed  
472 values. The average footprint emission sensitivities are shown in Figure 7 together with the  
473 locations of active fires in the last two months before the sample collection. The fire data  
474 were adopted from MODIS (Moderate Resolution Imaging Spectroradiometer) (Giglio et al.,  
475 2003) and the gas flaring facilities from the Global Gas Flaring Reduction Partnership  
476 (GGFR) (<http://www.worldbank.org/en/programs/gasflaringreduction>).

477 When the model strongly underestimated the measured EC ( $FB < -100\%$ ), the  
478 average footprint emission sensitivity showed the highest values over the Yamal Peninsula  
479 and the agglomeration of many gas flares in Khanty-Mansiysk (Figure 7 (b)). This might  
480 confirm the finding of Huang et al. (2014) that gas flaring emissions in the ECLIPSE  
481 inventory, while very high, are still underestimated. According to a related study by Huang  
482 and Fu (2016), Russia contributes 57% to the global BC emissions from gas flaring.  
483 Underestimation of modelled atmospheric concentrations compared to observations from the  
484 Barents and Kara Seas was recently also reported by Popovicheva et al. (2017), although the  
485 underestimation was relatively small.

486 When FLEXPART showed a moderate underestimation of EC concentrations in snow  
487 ( $-100\% < FB < 0\%$ ), the emission sensitivity was high near Arkhangelsk and over  
488 Scandinavia (Figure 7). BC emissions in Scandinavia are considered relatively low in most  
489 inventories and contribute no more than 6.5% to the global emissions in ACCMIP (Aerosol  
490 Chemistry Climate Model Intercomparison Project) (Lamarque et al., 2013), 6.2% in  
491 EDGARv4.2 (Emission Database for Global Atmospheric Research) (Olivier et al., 2005),  
492 2.1% in MACCity (Monitoring Atmospheric Composition & Climate / megaCITY - Zoom for  
493 the ENvironment) (Hollingsworth et al., 2008; Stein et al., 2012) and 3.3% in ECLIPSE  
494 (Klimont et al., 2016). The highest emission sensitivity was found over northwestern Russia  
495 (Figure 7), a region which includes Murmansk. Pollution levels in Murmansk could be high  
496 due to emissions from local industry, mining, heating and transport (Law and Stohl, 2007).

497 Another potential source region was Nenets/Komi area and Western Kazakhstan, where a few  
498 other flaring facilities are located (Figure 7).

499 Figure 7 shows that the underestimation of observed EC concentrations in snow  
500 strongly depends on the region, where samples are collected. In Western Siberia, the  
501 underestimation was larger than in northwestern European Russia. For this reason, we have  
502 computed the average region-specific emission sensitivities and the average region-specific  
503 contribution from the major polluting sources identified in ECLIPSE dataset. We distinguish  
504 between three regions, northwestern European Russia, Western Siberia (north of 62 °N) and  
505 Western Siberia (south of 62 °N) (Figure S 4 – S 6). For the samples collected in northwestern  
506 European Russia (Figure S 4), an average contribution of 21.6 ng g<sup>-1</sup> from all sources was  
507 estimated to have originated mainly from TRA (7.7 ng g<sup>-1</sup>) and DOM (10.4 ng g<sup>-1</sup>) sources in  
508 Finland. The contribution from BB and FLR emissions was insignificant (8% and 6%,  
509 respectively), whereas the rest of the ECLIPSE sources were negligible (IND, ENE, WST).  
510 For the samples collected at high latitudes in Western Siberia, the average contribution from  
511 all sources was more than 4 times higher (86 ng g<sup>-1</sup>) than those observed in northwestern  
512 European Russia (Figure S 5). FLR emissions accounted for 40% of the total contribution,  
513 which reflect the proximity of the sampling site to the main flaring facilities of Russia. The  
514 average contribution from TRA activities in Europe and southeastern Russia to the northern  
515 part of Western Siberia was 24%. Finally, DOM emissions in Eastern Europe also contributed  
516 another 28%. Finally, for the samples that were collected in the southern part of the Western  
517 Siberia an average contribution of 47.4 ng g<sup>-1</sup> was estimated from all sources included in  
518 ECLIPSE (Figure S 6). The highest contributing categories were TRA and DOM, whereas  
519 FLR appeared to contribute less, although the sampling site is close to Khanty-Mansiysk  
520 flaring region. This is attributed to the prevailing winds that forced flaring emissions to a  
521 northernmost direction opposite to the location of the sampling stations (see Figure S 6).

522 Overall, the region-specific analysis of the sources contributing to modelled BC in  
523 snow showed that the DOM, FLR and/or TRA sources might explain the model  
524 underestimation in high Arctic. However, in the most recent assessments of BC of the higher  
525 Arctic (Popovicheva et al., 2017; Winiger et al., 2017), it was shown that ECLIPSE captures  
526 levels of BC quite well, whereas FLR emissions might have a smaller impact in the Central  
527 Siberian Arctic (Tiksi) than previously estimated. Surprisingly, the average contribution from  
528 BB in lower latitudes was extremely low in all Western Siberia (Figure S 5 and S 6), despite  
529 the fact that sampling took place in springtime, where BB becomes important. Evangelidou et

530 al. (2016) reported that using a different dataset, that is based on the same approach as GFED,  
531 but includes updated emission factors for Eurasia, surface concentrations of BC in the Arctic  
532 stations can be substantially higher. This shows the need for further investigation of BC  
533 sources in the Russian Arctic.

## 534 **5 Conclusions**

535 We have analysed snow samples collected in Western Siberia and northwestern  
536 European Russia in 2014, 2015 and 2016 with respect to EC. This region is of major interest  
537 due to its large uncertainty in BC emissions and because it is located in the main transport  
538 route of BC to the Arctic. An effort to constrain the sources that contribute to measured  
539 concentration in BC in snow was made using the LPDM FLEXPART (version 10).

540 The observed EC levels in snow varied widely within and between regions (3–219 ng g<sup>-1</sup>  
541 <sup>1</sup> for 2014, 46–175 ng g<sup>-1</sup> in 2015 and 7–161 ng g<sup>-1</sup> in 2016), and are in the upper range of  
542 previously reported concentrations of EC and BC in snow in the Arctic region. However, the  
543 observed levels presented here appear typical for Western Siberia, which is subject to high  
544 domestic Russian emissions as well as to transport from distant European ones.

545 The snow BC concentrations predicted by the model are in a fair agreement with EC  
546 observations over Western Siberia and northwestern European Russia ( $R = 0.5 - 0.8$ ).  
547 However, the calculated negative MFB values (-48% to -27%) showed that the model  
548 systematically underestimated observations in Russia. This underestimation strongly  
549 depended on the region where the samples were collected. In northwestern European Russia,  
550 the main contributing sources were TRA and DOM mainly from adjacent regions in Finland.  
551 TRA and DOM contributed double to snow BC sampled at low latitudes of Western Siberia  
552 (<60°N) as compared to samples collected over regions above 60°N; the majority of these  
553 emissions originating from highly populated centres in Central Europe. Finally, in higher  
554 latitudes of Western Siberia (>60°N), snow BC concentrations were further increased mainly  
555 due to FLR emissions from facilities located close to the snow sampling points.

556 The modelled BC concentrations in snow were further investigated using two  
557 independent public measurement datasets that include samples from all over the Arctic for the  
558 period 2005 to 2009 and from Alert in 2014 and 2015. The model captured levels of BC fairly  
559 well despite the large variation in measured concentrations. An exception was observed in  
560 North America in spring 2007 and in Alert observatory in late winter – early spring 2015. In

561 both cases, the major sources were along the Canadian borders with USA and in Western  
562 Europe. Considering the fact that similar deviations were not observed in samples collected in  
563 the area during other years, it is likely that some of the prevailing sources of BC in this region  
564 show strong temporal variability in their emissions, and this is not taken into account in  
565 ECLIPSE inventory. Previously reported average measurements of BC concentrations in  
566 snow in Western Siberia and northwestern European Russia were  $80\pm 43$  ng g<sup>-1</sup>, which is  
567 about 30% higher than the EC measurements presented here ( $50\pm 46$  ng g<sup>-1</sup>).

568 **Data availability.** All data used for the present publication can be obtained from the  
569 corresponding author upon request.

570 **Competing interests.** The authors declare that they have no conflict of interest.

571 **Acknowledgements.** We would like to acknowledge the project entitled “Emissions of  
572 Short-Lived Climate Forcers near and in the Arctic (SLICFONIA)”, which was funded by the  
573 NORRUSS research program of the Research Council of Norway (Project ID: 233642) and  
574 the Russian Fund for Basic Research (project No. 15-05-08374) for funding snow sampling in  
575 the White Sea catchment area. We also thank Sergey Belorukov, Andrey Boev, Anton  
576 Bulokhov, Victor Drozdov, Sergey Kirpotin, Ivan Kritzkov, Rinat Manasypov, Ivan  
577 Semenyuk, and Alexander Yakovlev for helping during the three expeditions and  
578 Academician Alexander P. Lisitzin for his valuable recommendations. O. S. Pokrovsky and S.  
579 N. Vorobiev acknowledge support from BIO-GEO-CLIM grant No 14.B25.31.0001 for  
580 sampling in Western Siberia. Acknowledgements are also owed to IIASA (especially Chris  
581 Heyes and Zig Klimont) for providing the BC emission dataset. Computational and storage  
582 resources for the FLEXPART simulations have been provided by NOTUR (NN9419K) and  
583 NORSTORE (NS9419K). All plots from FLEXPART simulations have been included in an  
584 interactive website for fast visualization  
585 ([http://niflheim.nilu.no/NikolaosPY/SnowBC\\_141516.py](http://niflheim.nilu.no/NikolaosPY/SnowBC_141516.py)). All results can be accessed upon  
586 request to the corresponding author of this manuscript.

587 **Author Contributions.** N. Evangeliou designed and performed the modelling experiments  
588 and wrote the paper. V. P. Shevchenko organised and performed the sampling of EC, K.-E.  
589 Yttri performed all the TOA of the snow samples. S. Eckhardt modified FLEXPART model  
590 for the calculation of footprint emission sensitivities for deposited mass. E. Sollum wrote an  
591 algorithm that computes the starting date of the FLEXPART releases based on the water  
592 equivalent volume from ECMWF. O. S. Pokrovsky, V. O. Kobelev, V. B. Korobov, A. A.

593 Lobanov, D. P. Starodymova and S. N. Vorobiev assisted the sampling campaigns in Western  
594 Siberia and northwestern European Russia during 2014–2016. R. L. Thompson and A. Stohl  
595 supervised the study and wrote parts of the paper.

596

## 597 **References**

598 Aamaas, B., Bøggild, C. E., Stordal, F., Berntsen, T., Holmén, K. and Ström, J.: Elemental  
599 carbon deposition to Svalbard snow from Norwegian settlements and long-range transport,  
600 *Tellus, Ser. B Chem. Phys. Meteorol.*, 63(3), 340–351, doi:10.1111/j.1600-  
601 0889.2011.00531.x, 2011.

602 AMAP: AMAP assessment 2015: Black carbon and ozone as Arctic climate forcers, Arctic  
603 Monitoring and Assessment Programme (AMAP), Oslo, Norway., 2015.

604 Andreae, M. O. and Gelencsér, A.: Black carbon or brown carbon? The nature of light-  
605 absorbing carbonaceous aerosols, *Atmos. Chem. Phys.*, 6(3), 3419–3463, doi:10.5194/acpd-6-  
606 3419-2006, 2006.

607 Bond, T. C., Streets, D. G., Yarber, K. F., Nelson, S. M., Woo, J. H. and Klimont, Z.: A  
608 technology-based global inventory of black and organic carbon emissions from combustion, *J.*  
609 *Geophys. Res. D Atmos.*, 109(14), 1–43, doi:10.1029/2003JD003697, 2004.

610 Bond, T. C., Doherty, S. J., Fahey, D. W., Forster, P. M., Berntsen, T., Deangelo, B. J.,  
611 Flanner, M. G., Ghan, S., Kärcher, B., Koch, D., Kinne, S., Kondo, Y., Quinn, P. K., Sarofim,  
612 M. C., Schultz, M. G., Schulz, M., Venkataraman, C., Zhang, H., Zhang, S., Bellouin, N.,  
613 Guttikunda, S. K., Hopke, P. K., Jacobson, M. Z., Kaiser, J. W., Klimont, Z., Lohmann, U.,  
614 Schwarz, J. P., Shindell, D., Storelvmo, T., Warren, S. G. and Zender, C. S.: Bounding the  
615 role of black carbon in the climate system: A scientific assessment, *J. Geophys. Res. Atmos.*,  
616 118(11), 5380–5552, doi:10.1002/jgrd.50171, 2013.

617 Brandt, R. E., Warren, S. G., Worby, A. P. and Grenfell, T. C.: Surface albedo of the  
618 Antarctic sea ice zone, *J. Clim.*, 18(17), 3606–3622, doi:10.1175/JCLI3489.1, 2005.

619 Cavalli, F., Viana, M., Yttri, K. E., Genberg, J. and Putaud, J.-P.: Toward a standardised  
620 thermal-optical protocol for measuring atmospheric organic and elemental carbon: the  
621 EUSAAR protocol, *Atmos. Meas. Tech.*, 3(1), 79–89, doi:10.5194/amt-3-79-2010, 2010.



622 Cavalli, F., Putaud, J.-P. and Yttri, K. E.: Availability and quality of the EC and OC  
623 measurements within EMEP, including results of the fifth interlaboratory comparison of  
624 analytical methods for carbonaceous particulate matter within EMEP (2012)., 2015.

625 Clarke, A. D. and Noone, K. J.: Soot in the arctic snowpack: a cause for perturbations in  
626 radiative transfer, *Atmos. Environ.*, 41(SUPPL.), 64–72, doi:10.1016/0004-6981(85)90113-1,  
627 1985.

628 Doherty, S. J., Warren, S. G., Grenfell, T. C., Clarke, A. D. and Brandt, R. E.: Light-  
629 absorbing impurities in Arctic snow, *Atmos. Chem. Phys.*, 10(23), 11647–11680,  
630 doi:10.5194/acp-10-11647-2010, 2010.

631 Doherty, S. J., Grenfell, T. C., Forsström, S., Hegg, D. L., Brandt, R. E. and Warren, S. G.:  
632 Observed vertical redistribution of black carbon and other insoluble light-absorbing particles  
633 in melting snow, *J. Geophys. Res. Atmos.*, 118(11), 5553–5569, doi:10.1002/jgrd.50235,  
634 2013.

635 Eckhardt, S., Cassiani, M., Evangeliou, N., Sollum, E., Pisso, I. and Stohl, A.: Source-  
636 receptor matrix calculation for deposited mass with the Lagrangian particle dispersion model  
637 FLEXPART v10.2 in backward mode, *Geosci. Model Dev.*, 10, 4605–4618,  
638 doi:10.5194/gmd-10-4605-2017, 2017.

639 Evangeliou, N., Balkanski, Y., Hao, W. M., Petkov, A., Silverstein, R. P., Corley, R.,  
640 Nordgren, B. L., Urbanski, S. P., Eckhardt, S., Stohl, A., Tunved, P., Crepinsek, S., Jefferson,  
641 A., Sharma, S., Nøjgaard, J. K. and Skov, H.: Wildfires in northern Eurasia affect the budget  
642 of black carbon in the Arctic-a 12-year retrospective synopsis (2002-2013), *Atmos. Chem.*  
643 *Phys.*, 16(12), 7587–7604, doi:10.5194/acp-16-7587-2016, 2016.

644 Flanner, M. G., Zender, C. S., Randerson, J. T. and Rasch, P. J.: Present-day climate forcing  
645 and response from black carbon in snow, *J. Geophys. Res. Atmos.*, 112(11), 1–17,  
646 doi:10.1029/2006JD008003, 2007.

647 Forsström, S., Isaksson, E., Skeie, R. B., Ström, J., Pedersen, C. A., Hudson, S. R., Berntsen,  
648 T. K., Lihavainen, H., Godtlielsen, F. and Gerland, S.: Elemental carbon measurements in  
649 European Arctic snow packs, *J. Geophys. Res. Atmos.*, 118(24), 13614–13627,  
650 doi:10.1002/2013JD019886, 2013.

651 Forster, C., Wandinger, U., Wotawa, G., James, P., Mattis, I., Althausen, D., Simmonds, P.,

652 O'Doherty, S., Jennings, S. G., Kleefeld, C., Schneider, J., Trickl, T., Kreipl, S., Jäger, H. and  
653 Stohl, A.: Transport of boreal forest fire emissions from Canada to Europe, *J. Geophys. Res.*,  
654 106, 22887, doi:10.1029/2001JD900115, 2001.

655 Giglio, L., Descloitres, J., Justice, C. O. and Kaufman, Y. J.: An enhanced contextual fire  
656 detection algorithm for MODIS, *Remote Sens. Environ.*, 87(2–3), 273–282,  
657 doi:10.1016/S0034-4257(03)00184-6, 2003.

658 Giglio, L., Randerson, J. T. and van der Werf, G. R.: Analysis of daily, monthly, and annual  
659 burned area using the fourth-generation global fire emissions database (GFED4), *J. Geophys.*  
660 *Res. Biogeosciences*, 118, 317–328, doi:10.1002/jgrg.20042, 2013, 2013.

661 Grythe, H., Kristiansen, N. I., Groot Zwaaftink, C. D., Eckhardt, S., Ström, J., Tunved, P.,  
662 Krejci, R. and Stohl, A.: A new aerosol wet removal scheme for the Lagrangian particle  
663 model FLEXPARTv10, *Geosci. Model Dev.*, 10, 1447–1466, doi:10.5194/gmd-10-1447-  
664 2017, 2017.

665 Hadley, O. L., Corrigan, C. E., Kirchstetter, T. W., Cliff, S. S. and Ramanathan, V.: Measured  
666 black carbon deposition on the Sierra Nevada snow pack and implication for snow pack  
667 retreat, *Atmos. Chem. Phys.*, 10(15), 7505–7513, doi:10.5194/acp-10-7505-2010, 2010.

668 Hansen, J. and Nazarenko, L.: Soot climate forcing via snow and ice albedos, *Proc. Natl.*  
669 *Acad. Sci. U. S. A.*, 101(2), 423–428, doi:10.1073/pnas.2237157100, 2004.

670 Hao, W. M., Petkov, A., Nordgren, B. L., Silverstein, R. P., Corley, R. E., Urbanski, S. P.,  
671 Evangeliou, N., Balkanski, Y. and Kinder, B.: Daily black carbon emissions from fires in  
672 Northern Eurasia from 2002 to 2013, *Geosci. Model Dev. Discuss.*, (April), 1–24,  
673 doi:10.5194/gmd-2016-89, 2016.

674 Hegg, D. A., Warren, S. G., Grenfell, T. C., Doherty, S. J., Larson, T. V. and Clarke, A. D.:  
675 Source attribution of black carbon in arctic snow, *Environ. Sci. Technol.*, 43(11), 4016–4021,  
676 doi:10.1021/es803623f, 2009.

677 Hegg, D. A., Warren, S. G., Grenfell, T. C., Doherty, S. J. and Clarke, A. D.: Sources of light-  
678 absorbing aerosol in arctic snow and their seasonal variation, *Atmos. Chem. Phys.*, 10(22),  
679 10923–10938, doi:10.5194/acp-10-10923-2010, 2010.

680 Hollingsworth, A., Engelen, R. J., Textor, C., Benedetti, A., Boucher, O., Chevallier, F.,

681 Dethof, A., Elbern, H., Eskes, H., Flemming, J., Granier, C., Kaiser, J. W., Morcrette, J. J.,  
682 Rayner, P., Peuch, V. H., Rouil, L., Schultz, M. G. and Simmons, A. J.: Toward a monitoring  
683 and forecasting system for atmospheric composition: The GEMS project, *Bull. Am. Meteorol.*  
684 *Soc.*, 89(8), 1147–1164, doi:10.1175/2008BAMS2355.1, 2008.

685 Huang, K. and Fu, J. S.: Data Descriptor : A global gas flaring black carbon emission rate  
686 dataset from 1994 to 2012, *Nature*, 1–11, doi:10.1038/sdata.2016.104, 2016.

687 Huang, K., Fu, J. S., Hodson, E. L., Dong, X., Cresko, J., Prikhodko, V. Y., Storey, J. M. and  
688 Cheng, M. D.: Identification of missing anthropogenic emission sources in Russia:  
689 Implication for modeling arctic haze, *Aerosol Air Qual. Res.*, 14(7), 1799–1811,  
690 doi:10.4209/aaqr.2014.08.0165, 2014.

691 Ingvander, S., Rosqvist, G., Svensson, J. and Dahlke, H. E.: Seasonal and interannual  
692 variability of elemental carbon in the snowpack of Storglaci??ren, northern Sweden, *Ann.*  
693 *Glaciol.*, 54(62), 50–58, doi:10.3189/2013AoG62A229, 2013.

694 Jankowski, N., Schmidl, C., Marr, I. L., Bauer, H. and Puxbaum, H.: Comparison of methods  
695 for the quantification of carbonate carbon in atmospheric PM10 aerosol samples, *Atmos.*  
696 *Environ.*, 42(34), 8055–8064, doi:10.1016/j.atmosenv.2008.06.012, 2008.

697 Klimont, Z., Kupiainen, K., Heyes, C., Purohit, P., Cofala, J., Rafaj, P., Borken-Kleefeld, J.  
698 and Schöpp, W.: Global anthropogenic emissions of particulate matter including black  
699 carbon, *Atmos. Chem. Phys. Discuss.*, (October), 1–72, doi:10.5194/acp-2016-880, 2016.

700 Lamarque, J. F., Shindell, D. T., Josse, B., Young, P. J., Cionni, I., Eyring, V., Bergmann, D.,  
701 Cameron-Smith, P., Collins, W. J., Doherty, R., Dalsoren, S., Faluvegi, G., Folberth, G.,  
702 Ghan, S. J., Horowitz, L. W., Lee, Y. H., MacKenzie, I. A., Nagashima, T., Naik, V.,  
703 Plummer, D., Righi, M., Rumbold, S. T., Schulz, M., Skeie, R. B., Stevenson, D. S., Strode,  
704 S., Sudo, K., Szopa, S., Voulgarakis, A. and Zeng, G.: The atmospheric chemistry and climate  
705 model intercomparison Project (ACCMIP): Overview and description of models, simulations  
706 and climate diagnostics, *Geosci. Model Dev.*, 6(1), 179–206, doi:10.5194/gmd-6-179-2013,  
707 2013.

708 Law, K. S. and Stohl, A.: Arctic Air Pollution: Origins and Impacts, *Science* (80-. ),  
709 315(5818), 1537–1540, doi:10.1126/science.1137695, 2007.

710 Lelieveld, J., Evans, J. S., Fnais, M., Giannadaki, D. and Pozzer, A.: The contribution of

711 outdoor air pollution sources to premature mortality on a global scale., *Nature*, 525(7569),  
712 367–71, doi:10.1038/nature15371, 2015.

713 Liu, J., Fan, S., Horowitz, L. W. and Levy, H.: Evaluation of factors controlling long-range  
714 transport of black carbon to the Arctic, *J. Geophys. Res.*, 116(D4), D04307,  
715 doi:10.1029/2010JD015145, 2011.

716 Macdonald, K. M., Sharma, S., Toom, D., Chivulescu, A., Hanna, S., Bertram, A., Platt, A.,  
717 Elsasser, M., Huang, L., Chellman, N., McConnell, J. R., Bozem, H., Kunkel, D., Lei, Y. D.,  
718 Evans, G. J. and Abbatt, J. P. D.: Observations of Atmospheric Chemical Deposition to High  
719 Arctic Snow, *Atmos. Chem. Phys.*, 17, 5775–5788, doi:10.5194/acp-17-5775-2017, 2017.

720 McConnell, J. R., Edwards, R., Kok, G. L., Flanner, M. G., Zender, C. S., Saltzman, E. S.,  
721 Banta, J. R., Pasteris, D. R., Carter, M. M. and Kahl, J. D. W.: 20th-Century Industrial Black  
722 Carbon Emissions Altered Arctic Climate Forcing, *Science* (80-. ), 317(5843), 1381–1384,  
723 doi:10.1126/science.1144856, 2007.

724 Ogren, J. A., Charlson, R. J. and Groblicki, P. J.: Determination of elemental carbon in  
725 rainwater, *Anal. Chem.*, 55(9), 1569–1572, doi:10.1021/ac00260a027, 1983.

726 Olivier, J. G. J., Aardenne, J. A. Van, Dentener, F. J., Pagliari, V., Ganzeveld, L. N. and  
727 Peters, J. A. H. W.: Recent trends in global greenhouse gas emissions: regional trends 1970–  
728 2000 and spatial distribution of key sources in 2000, *Environ. Sci.*, 2(2–3), 81–99,  
729 doi:10.1080/15693430500400345, 2005.

730 Petzold, A., Ogren, J. A., Fiebig, M., Laj, P., Li, S. M., Baltensperger, U., Holzer-Popp, T.,  
731 Kinne, S., Pappalardo, G., Sugimoto, N., Wehrli, C., Wiedensohler, A. and Zhang, X. Y.:  
732 Recommendations for reporting black carbon measurements, *Atmos. Chem. Phys.*, 13(16),  
733 8365–8379, doi:10.5194/acp-13-8365-2013, 2013.

734 Popovicheva, O. B., Evangelidou, N., Eleftheriadis, K., Kalogridis, A. C., Movchan, V.,  
735 Sitnikov, N., Eckhardt, S., Makshtas, A. and Stohl, A.: Black carbon sources constrained by  
736 observations and modeling in the Russian high Arctic, *Environ. Sci. Technol.*, submitted,  
737 doi:10.1021/acs.est.6b05832, 2017.

738 Qi, L., Li, Q., Henze, D. K., Tseng, H.-L. and He, C.: Sources of Springtime Surface Black  
739 Carbon in the Arctic: An Adjoint Analysis, *Atmos. Chem. Phys. Discuss.*, (February), 1–32,  
740 doi:10.5194/acp-2016-1112, 2017.

741 Ruppel, M. M., Isaksson, I., Ström, J., Beaudon, E., Svensson, J., Pedersen, C. A. and  
742 Korhola, A.: Increase in elemental carbon values between 1970 and 2004 observed in a 300-  
743 year ice core from Holtedahlfonna (Svalbard), *Atmos. Chem. Phys.*, 14(20), 11447–11460,  
744 doi:10.5194/acp-14-11447-2014, 2014.

745 Sand, M., Berntsen, T. K., von Salzen, K., Flanner, M. G., Langner, J. and Victor, D. G.:  
746 Response of Arctic temperature to changes in emissions of short-lived climate forcers, *Nat.*  
747 *Clim. Chang.*, 6(November), 1–5, doi:10.1038/nclimate2880, 2015.

748 Seibert, P. and Frank, A.: Source-receptor matrix calculation with a Lagrangian particle  
749 dispersion model in backward mode, *Atmos. Chem. Phys.*, 4(1), 51–63, doi:10.5194/acp-4-  
750 51-2004, 2004.

751 Sharma, S., Ishizawa, M., Chan, D., Lavoué, D., Andrews, E., Eleftheriadis, K. and  
752 Maksyutov, S.: 16-year simulation of arctic black carbon: Transport, source contribution, and  
753 sensitivity analysis on deposition, *J. Geophys. Res. Atmos.*, 118(2), 943–964,  
754 doi:10.1029/2012JD017774, 2013.

755 Shiraiwa, M., Kondo, Y., Moteki, N., Takegawa, N., Sahu, L. K., Takami, A., Hatakeyama,  
756 S., Yonemura, S. and Blake, D. R.: Radiative impact of mixing state of black carbon aerosol  
757 in Asian outflow, *J. Geophys. Res. Atmos.*, 113(24), 1–13, doi:10.1029/2008JD010546, 2008.

758 Silverstein, J. C., Parsad, N. M. and Tsirline, V.: NIH Public Access, , 41(6), 927–935,  
759 doi:10.1016/j.jbi.2008.02.008.Automatic, 2009.

760 Singh, P. and Haritashya, U. K.: *Encyclopedia of Snow, Ice and Glaciers.*, 2011.

761 Slinn, W. G. N.: Predictions for particle deposition to vegetative canopies, *Atmos. Environ.*,  
762 16, 1785–1794, doi:10.1016/0004-6981(82)90271-2, 1982.

763 Stein, O., Flemming, J., Inness, A., Kaiser, J. W. and Schultz, M. G.: Global reactive gases  
764 forecasts and reanalysis in the MACC project, *J. Integr. Environ. Sci.*, 8168(October 2014),  
765 1–14, doi:10.1080/1943815X.2012.696545, 2012.

766 Stohl, A., Hittenberger, M. and Wotawa, G.: Validation of the lagrangian particle dispersion  
767 model FLEXPART against large-scale tracer experiment data, *Atmos. Environ.*, 32(24),  
768 4245–4264, doi:10.1016/S1352-2310(98)00184-8, 1998.

769 Stohl, A., Forster, C., Eckhardt, S., Spichtinger, N., Huntrieser, H., Heland, J., Schlager, H.,

770 Wilhelm, S., Arnold, F. and Cooper, O.: A backward modeling study of intercontinental  
771 pollution transport using aircraft measurements, *J. Geophys. Res. Atmos.*, 108(D12), 4370,  
772 doi:10.1029/2002JD002862, 2003.

773 Stohl, A., Forster, C., Frank, A., Seibert, P. and Wotawa, G.: Technical note: The Lagrangian  
774 particle dispersion model FLEXPART version 6.2, *Atmos. Chem. Phys.*, 5(9), 2461–2474,  
775 doi:10.5194/acp-5-2461-2005, 2005.

776 Stohl, A., Andrews, E., Burkhardt, J. F., Forster, C., Herber, A., Hoch, S. W., Kowal, D.,  
777 Lunder, C., Mefford, T., Ogren, J. A., Sharma, S., Spichtinger, N., Stebel, K., Stone, R.,  
778 Ström, J., Tørseth, K., Wehrli, C. and Yttri, K. E.: Pan-Arctic enhancements of light  
779 absorbing aerosol concentrations due to North American boreal forest fires during summer  
780 2004, *J. Geophys. Res. Atmos.*, 111(22), 1–20, doi:10.1029/2006JD007216, 2006.

781 Stohl, A., Klimont, Z., Eckhardt, S., Kupiainen, K., Shevchenko, V. P., Kopeikin, V. M. and  
782 Novigatsky, A. N.: Black carbon in the Arctic: The underestimated role of gas flaring and  
783 residential combustion emissions, *Atmos. Chem. Phys.*, 13(17), 8833–8855, doi:10.5194/acp-  
784 13-8833-2013, 2013.

785 Stohl, A., Aamaas, B., Amann, M., Baker, L. H., Bellouin, N., Berntsen, T. K., Boucher, O.,  
786 Cherian, R., Collins, W., Daskalakis, N., Dusinska, M., Eckhardt, S., Fuglestvedt, J. S., Harju,  
787 M., Heyes, C., Hodnebrog, Hao, J., Im, U., Kanakidou, M., Klimont, Z., Kupiainen, K., Law,  
788 K. S., Lund, M. T., Maas, R., MacIntosh, C. R., Myhre, G., Myriokefalitakis, S., Olivie, D.,  
789 Quaas, J., Quennehen, B., Raut, J. C., Rumbold, S. T., Samset, B. H., Schulz, M., Seland,  
790 Shine, K. P., Skeie, R. B., Wang, S., Yttri, K. E. and Zhu, T.: Evaluating the climate and air  
791 quality impacts of short-lived pollutants, *Atmos. Chem. Phys.*, 15(18), 10529–10566,  
792 doi:10.5194/acp-15-10529-2015, 2015.

793 Svensson, J., Ström, J., Hansson, M., Lihavainen, H. and Kerminen, V.-M.: Observed metre  
794 scale horizontal variability of elemental carbon in surface snow, *Environ. Res. Lett.*, 8(3),  
795 34012, doi:10.1088/1748-9326/8/3/034012, 2013.

796 Turner, M. D., Henze, D. K., Capps, S. L., Hakami, A., Zhao, S., Resler, J., Carmichael, G.  
797 R., Stanier, C. O., Baek, J., Sandu, A., Russell, A. G., Nenes, A., Pinder, R. W., Napelenok, S.  
798 L., Bash, J. O., Percell, P. B. and Chai, T.: Premature deaths attributed to source-specific BC  
799 emissions in six urban US regions, , 10(114014), doi:10.1088/1748-9326/10/11/114014/meta,  
800 2005.

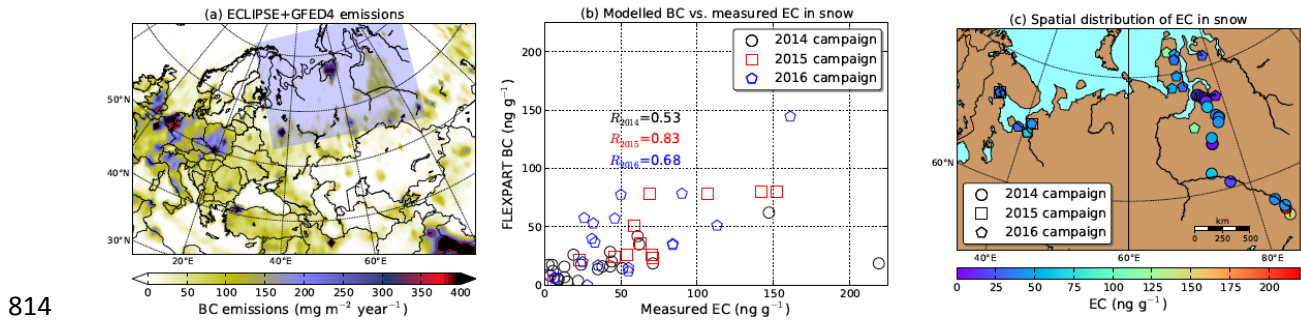
801 Wang, Q., Jacob, D. J., Fisher, J. A., Mao, J., Leibensperger, E. M., Carouge, C. C., Le Sager,  
802 P., Kondo, Y., Jimenez, J. L., Cubison, M. J. and Doherty, S. J.: Sources of carbonaceous  
803 aerosols and deposited black carbon in the Arctic in winter-spring: Implications for radiative  
804 forcing, *Atmos. Chem. Phys.*, 11(23), 12453–12473, doi:10.5194/acp-11-12453-2011, 2011.

805 Warren, S. G. and Wiscombe, W. J.: A Model for the Spectral Albedo of Snow. II: Snow  
806 Containing Atmospheric Aerosols, *J. Atmos. Sci.*, 37, 2734–2745, doi:10.1175/1520-  
807 0469(1980)037<2734:AMFTSA>2.0.CO;2, 1980.

808 Winiger, P., Andersson, A., Eckhardt, S., Stohl, A., Semiletov, I. P., Dudarev, O. V., Charkin,  
809 A., Shakhova, N., Klimont, Z., Heyes, C. and Gustafsson, Ö.: Siberian Arctic black carbon  
810 sources constrained by model and observation, *Proc. Natl. Acad. Sci.*, 1–8,  
811 doi:10.1073/pnas.1613401114, 2017.

812

813 **FIGURE CAPTIONS FOR MANUSCRIPT**

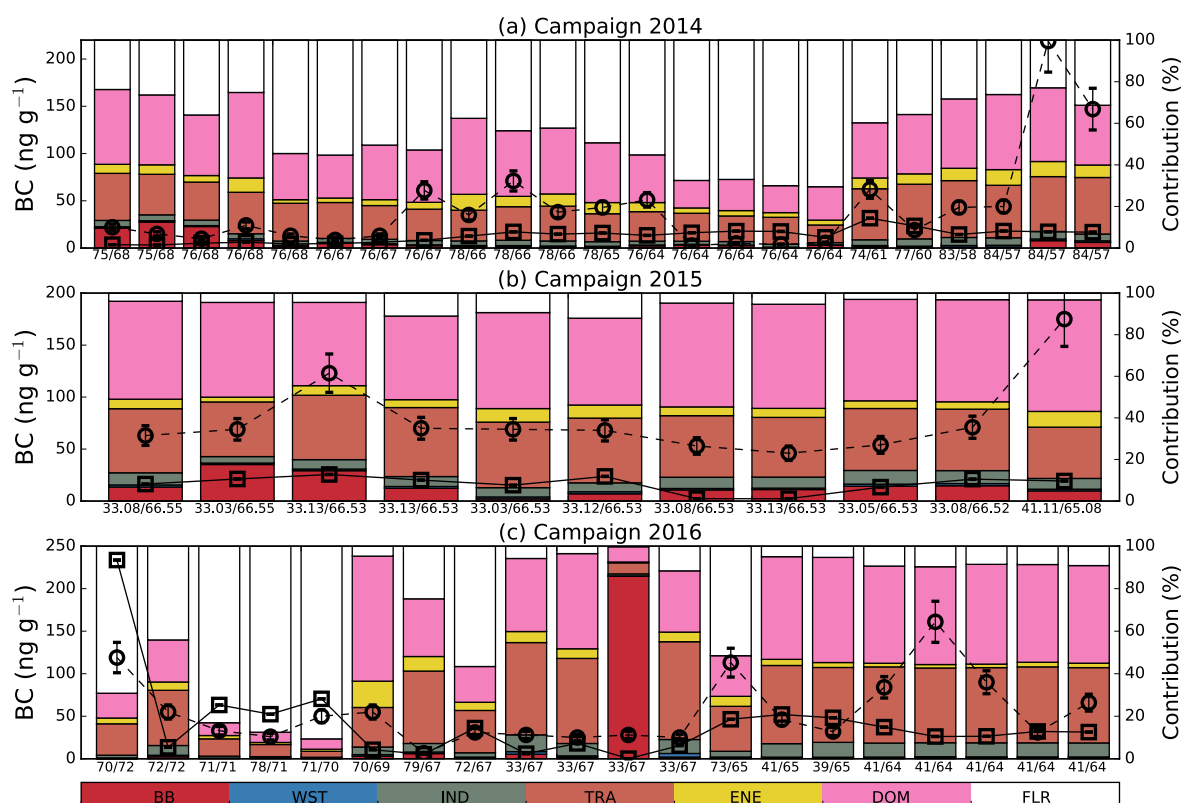


815 **Figure 1.** (a) Total emissions of BC (anthropogenic emissions from ECLIPSE (Klimont et al.,  
 816 2016) and biomass burning from GFED4 (Giglio et al., 2013)). The blue shade shows the area  
 817 of interest that is zoomed on the right. (b) Comparison of modelled BC concentrations in  
 818 snow with measured EC concentrations. (c) Spatial distribution of EC in snow measured by  
 819 thermal optical analysis (TOA) of filtered snow samples from northwestern European Russia  
 820 and Western Siberia in spring–time 2014, 2015 and 2016 (Silverstein et al., 2009).

821



## SOURCE CONTRIBUTION TO SNOW BC

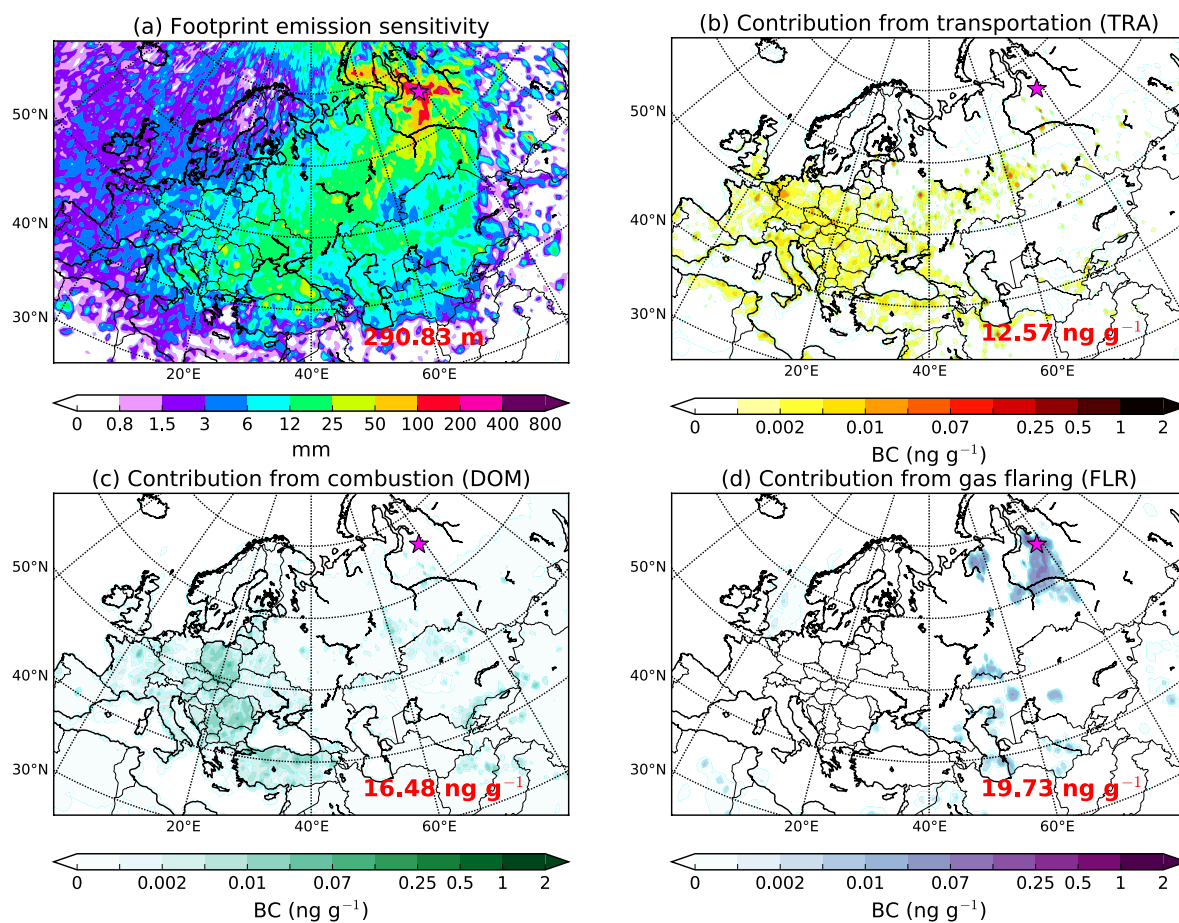


822

823 **Figure 2.** Contribution from the various emission categories considered in the ECLIPSE and  
 824 GFED inventories to simulated BC concentrations in snow in (a) 2014, (b) 2015 and (c) 2016  
 825 in Western Siberia and northwestern European Russia. BB stands for biomass burning, WST  
 826 for waste burning, IND for industrial combustion and processing, TRA for surface  
 827 transportation, ENE for emissions from energy conversion, and extraction, DOM for  
 828 residential and commercial combustion, and FLR for gas flaring. Bars show the relative  
 829 source contribution (0 –100%, right axis) and are sorted, from left to right, from the  
 830 northernmost to the southernmost measurement location (coordinates are reported on the  
 831 bottom as longitude/latitude). Measured EC concentrations in snow are reported with open  
 832 circles, whereas modelled BC is shown with open rectangles (left axis).

833

**EMISSION SENSITIVITY AND SOURCE CONTRIBUTION TO SNOW BC IN 2014  
(78.17° E - 65.78° N)**

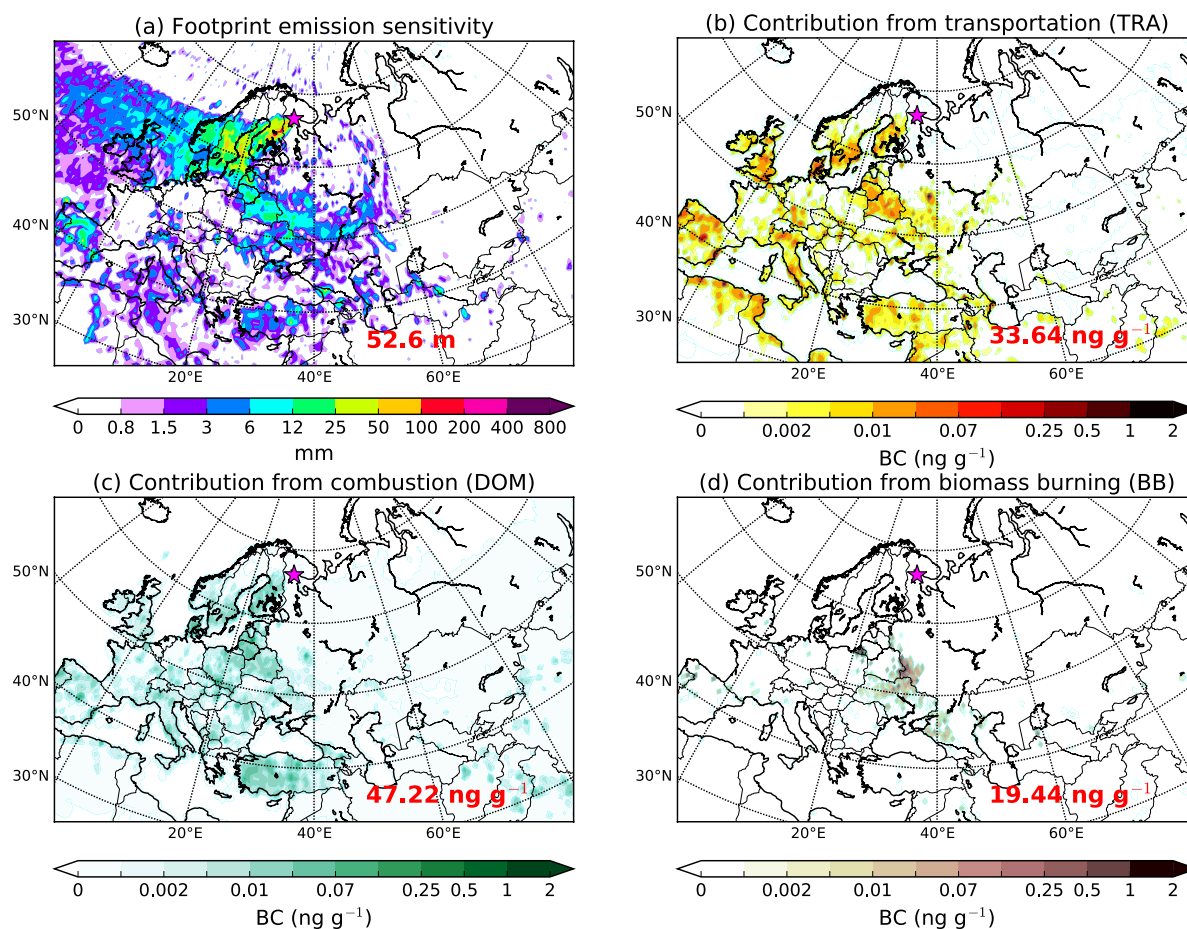


834

835 **Figure 3.** (a) FLEXPART emission sensitivity, contribution from (b) transportation (TRA),  
 836 (c) residential and commercial combustion (DOM) and (d) gas flaring (FLR) to the maximum  
 837 measured concentration of snow EC recorded along the transect from Tomsk to Yamal  
 838 Peninsula in Western Siberia during the campaign of 2014.

839

**EMISSION SENSITIVITY AND SOURCE CONTRIBUTION TO SNOW BC IN 2015  
(33.13° E - 66.53° N)**

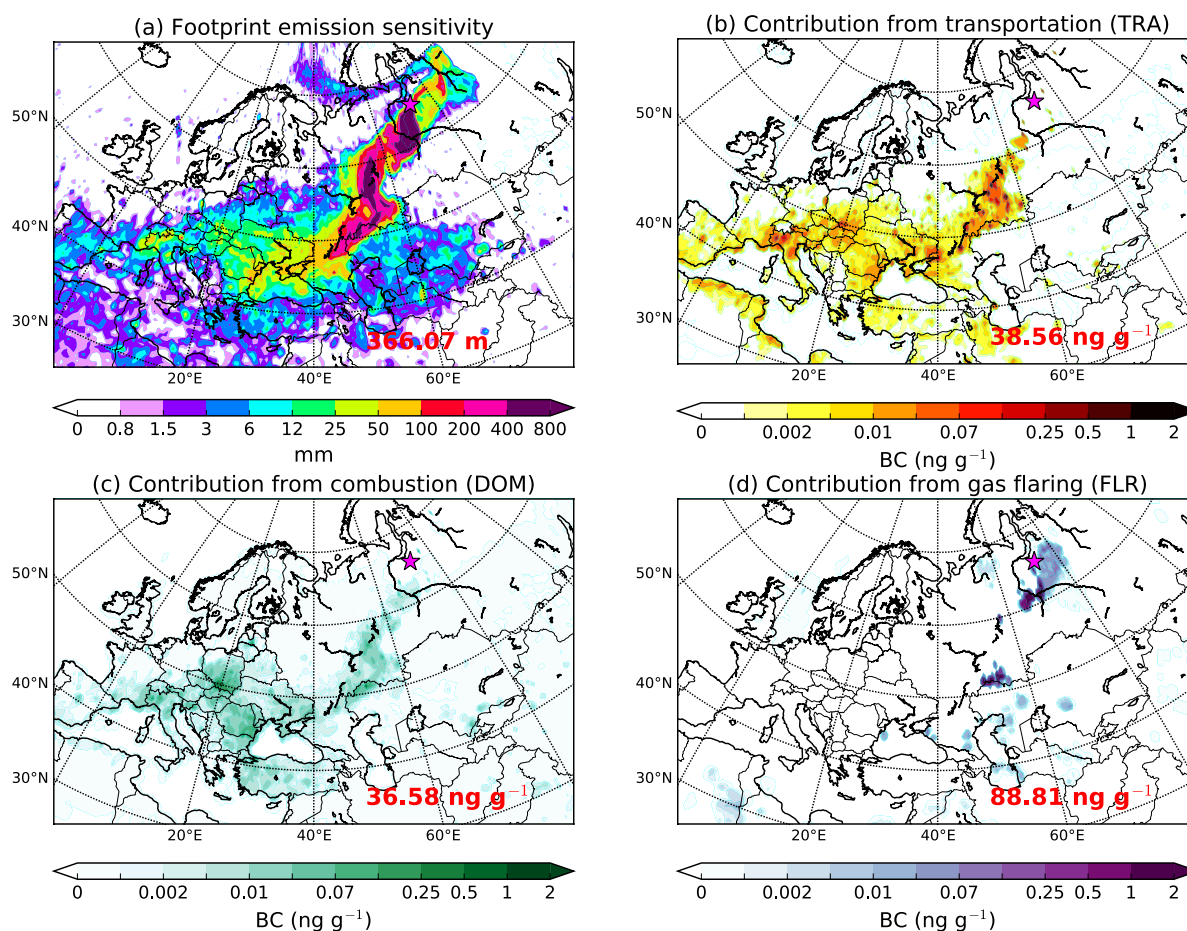


840

841 **Figure 4.** (a) FLEXPART emission sensitivity, (b) contribution from transportation (TRA),  
 842 (c) residential and commercial combustion (DOM) and (d) gas flaring (FLR) to the maximum  
 843 measured concentration of snow EC recorded in northwestern European Russia (Kindo  
 844 Peninsula and Arkhangelsk region) during the campaign of 2015.

845

**EMISSION SENSITIVITY AND SOURCE CONTRIBUTION TO SNOW BC IN 2016  
(72.94° E - 65.36° N)**

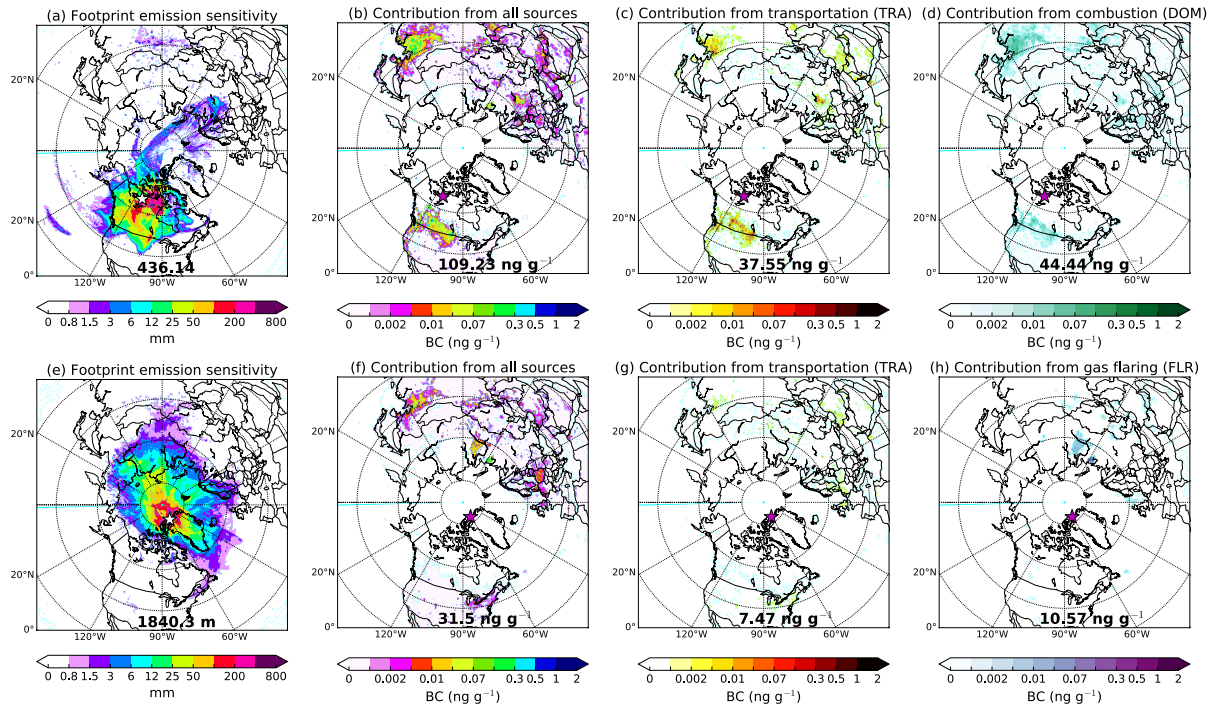


846

847 **Figure 5.** (a) FLEXPART emission sensitivity and (b) contribution from transportation  
 848 (TRA), (c) residential and commercial combustion (DOM) and (d) gas flaring (FLR) to the  
 849 maximum measured concentration of snow EC recorded in Kindo Peninsula, Arkhangelsk and  
 850 Yamal Peninsula (northwestern European Russia, Western Siberia) during the campaign of  
 851 2016.

852

**EMISSION SENSITIVITY AND SOURCE CONTRIBUTION TO SNOW BC  
(CANADIAN ARCTIC 2007 - ALERT 2014-2015)**



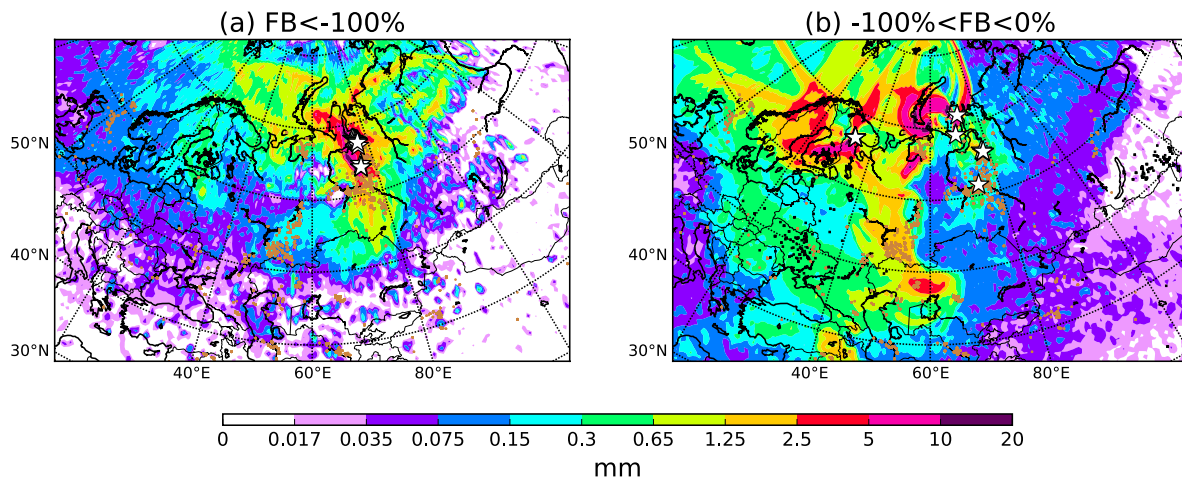
853

854 **Figure 6.** (a–d) Footprint emission sensitivity and major contribution from all sources, TRA  
 855 and DOM averaged for the samples that showed overestimated modelled concentrations of  
 856 BC in 2007 (Doherty et al., 2010). (e–h) Footprint emission sensitivity and contribution from  
 857 all sources, TRA and FLR for the samples collected in Alert (Macdonald et al., 2017) that  
 858 model overestimated by more than three times.

859



**AVERAGE FOOTPRINT EMISSION SENSITIVITY  
NORMALISED AGAINST UNDERESTIMATION FROM OBSERVATIONS**



860

861 **Figure 7.** (a) Footprint emission sensitivity from FLEXPART averaged for the sampling  
862 points where the model underestimated observations significantly ( $FB < -100\%$ ) and (b)  
863 less significantly ( $-100\% < FB < 0\%$ ). Black squares show the locations of active fires  
864 detected by MODIS (Moderate Resolution Imaging Spectroradiometer) (Giglio et al., 2003).  
865 Brown dots show the location of gas flaring sites from the Global Gas Flaring Reduction  
866 Partnership (GGFR) (<http://www.worldbank.org/en/programs/gasflaringreduction>).

867

868 **FIGURE & TABLE CAPTIONS FOR SUPPLEMENTS**

869

870 **Figure S 1.** Fractional bias ( $FB = [(C_m - C_o)/(C_m + C_o) \times 0.5] \times 100\%$ ) for all samples  
871 collected from the three campaigns in Western Siberia and northwestern European Russia in  
872 2014, 2015 and 2016. MFB (mean fractional bias) is the fractional bias averaged for all snow  
873 samples from 2014, 2015 and 2016, whereas RMSE is the root mean square error in  $ng\ g^{-1}$ ).

874 **Figure S 2.** (a) Distribution of snow measurements of BC adopted from Doherty et al. (2010)  
875 in the Arctic from 2005 to 2009. (b) Simulated (FLEXPART) BC concentrations in snow for  
876 the same period (right). MFB, RMSE and correlation coefficient (R) values are further given.

877 **Figure S 3.** Timeseries of simulated and measured BC concentrations in snow collected in  
878 Alert (Macdonald et al., 2017). Correlation coefficient (R) between modelled and measured  
879 BC, RMSE and MFB values are also shown.

880 **Figure S 4.** (a) Average footprint emission sensitivity and (b–f) source contribution (from all  
881 sources, TRA, DOM, FLR and BB) for all the samples located in northwestern European  
882 Russia.

883 **Figure S 5.** (a) Average footprint emission sensitivity and (b–f) source contribution (from all  
884 sources, TRA, DOM, FLR and BB) for all the samples located in Western Siberia (north of 62  
885 °N).

886 **Figure S 6.** (a) Average footprint emission sensitivity and (b–f) source contribution (from all  
887 sources, TRA, DOM, FLR and BB) for all the samples located in Western Siberia (south of  
888 62 °N).

889

890 **Table S 1.** Information about the samples collected in springtime of 2014, 2015 and 2016 in  
891 Western Russia.

892

893 **Table S 2.**  $EC_{CO_3}^{corr}$  to  $EC$  ratio (Mean  $\pm$  SD; Min - Max), showing overestimation of  $EC$  due  
894 to  $EC_{CO_3}$  in the filtered snow samples.